

Review

# Progress and Perspectives of Spectroscopic Studies on Carbon K-Edge Using Novel Soft X-ray Pulsed Sources

Zeinab Ebrahimpour <sup>1,\*</sup>, Marcello Coreno <sup>1,2</sup>, Luca Giannessi <sup>1,3</sup>, Massimo Ferrario <sup>1</sup>, Augusto Marcelli <sup>1,4,5</sup>, Federico Nguyen <sup>6</sup>, Seyed Javad Rezvani <sup>1,7</sup>, Francesco Stellato <sup>8,9</sup> and Fabio Villa <sup>1</sup>

<sup>1</sup> Laboratori Nazionali di Frascati, INFN, Via E. Fermi 54, 00044 Frascati, Italy

<sup>2</sup> Istituto Struttura della Materia and Elettra-Sincrotrone Trieste, CNR, Basovizza Area Science Park, 34149 Trieste, Italy

<sup>3</sup> Elettra-Sincrotrone Trieste, Basovizza Area Science Park, 34149 Trieste, Italy

<sup>4</sup> International Center for Material Science Superstripes, RICMASS, Via dei Sabelli 119A, 00185 Rome, Italy

<sup>5</sup> Istituto Struttura della Materia, CNR, Via del Fosso del Cavaliere 100, 00133 Rome, Italy

<sup>6</sup> Fusion and Nuclear Safety Department, ENEA C.R. Frascati, Via E. Fermi 45, 00044 Frascati, Italy

<sup>7</sup> Physics Division, School of Science and Technology, Università di Camerino, Via Madonna delle Carceri 9, 62032 Camerino, Italy

<sup>8</sup> Physics Department, University of Rome Tor Vergata, Via della Ricerca Scientifica 1, 00133 Roma, Italy

<sup>9</sup> INFN—Sezione di Roma Tor Vergata, Via della Ricerca Scientifica 1, 00133 Roma, Italy

\* Correspondence: zeinab.ebrahimpour@lnf.infn.it

**Abstract:** The development of novel coherent and brilliant sources, such as soft X-ray free electron laser (FEL) and high harmonic generation (HHG), enables new ultrafast analysis of the electronic and structural dynamics of a wide variety of materials. Soft X-ray FEL delivers high-brilliance beams with a short pulse duration, high spatial coherence and photon energy tunability. In comparison with FELs, HHG X-ray sources are characterized by a wide spectral bandwidth and few- to sub-femtosecond pulses. The approach will lead to the time-resolved reconstruction of molecular dynamics, shedding light on different photochemical pathways. The high peak brilliance of soft X-ray FELs facilitates investigations in a nonlinear regime, while the broader spectral bandwidth of the HHG sources may provide the simultaneous probing of multiple components. Significant technical breakthroughs in these novel sources are under way to improve brilliance, pulse duration, and to control spectral bandwidth, spot size, and energy resolution. Therefore, in the next few years, the new generation of soft X-ray sources combined with novel experimental techniques, new detectors, and computing capabilities will allow for the study of several extremely fast dynamics, such as vibronic dynamics. In the present review, we discuss recent developments in experiments, performed with soft X-ray FELs and HHG sources, operating near the carbon K-absorption edge, being a key atomic component in biosystems and soft materials. Different spectroscopy methods such as time-resolved pump-probe techniques, nonlinear spectroscopies and photoelectron spectroscopy studies have been addressed in an attempt to better understand fundamental physico-chemical processes.

**Keywords:** soft X-ray FEL; HHG pulses; time-resolved X-ray spectroscopy; carbon K-edge; conical intersections; EuPRAXIA@SPARC\_LAB



**Citation:** Ebrahimpour, Z.; Coreno, M.; Giannessi, L.; Ferrario, M.; Marcelli, A.; Nguyen, F.; Rezvani, S.J.; Stellato, F.; Villa, F. Progress and Perspectives of Spectroscopic Studies on Carbon K-Edge Using Novel Soft X-ray Pulsed Sources. *Condens. Matter* **2022**, *7*, 72. <https://doi.org/10.3390/condmat7040072>

Academic Editor: Andreas Germanos Karydas

Received: 9 November 2022

Accepted: 2 December 2022

Published: 6 December 2022

**Publisher's Note:** MDPI stays neutral with regard to jurisdictional claims in published maps and institutional affiliations.



**Copyright:** © 2022 by the authors. Licensee MDPI, Basel, Switzerland. This article is an open access article distributed under the terms and conditions of the Creative Commons Attribution (CC BY) license (<https://creativecommons.org/licenses/by/4.0/>).

## 1. Introduction

X-ray spectroscopy is one of the fundamental spectroscopic techniques in material science due to its element and site selectivity in providing information on local structural and electronic configurations and properties [1–7]. For instance, the large binding energy difference of the carbon (C), nitrogen (N), and oxygen (O) core level electrons (about 100 eV) can be easily resolved with existing spectrometers, allowing for the investigation of structural and/or electronic dynamics of the materials containing these elements. The capability to probe core-electronic states and unoccupied valence/Rydberg states makes core-level spectroscopy a

unique tool for probing and recognizing features of different molecules, including excited-state lifetimes, electronic energies, vibrational distributions, and spin states.

Soft X-rays in the range from 1 to 10 nm ( $\approx 1240$ – $124$  eV) are particularly suited for investigating linear and nonlinear effects in biomaterials, nanomaterials, polymers, and organic molecules. X-ray spectroscopy in the soft X-ray energies represents a wonderful tool for dynamical and structural analysis. Many technological materials widely used in industrial applications are made of light elements such as C, N, and O atoms, all of which have their K-absorption edge in the soft X-ray energy range. Among them, carbon is a key element of bio-materials and the major component of soft materials. Moreover, after the creation of the core-hole, C K-edge absorption spectra are characterized by sharper features and a high spectral contrast because of their longer core-hole lifetime and small vibrational broadening, a great advantage in comparison to spectroscopy at the O and N K-edges [8].

In order to study ultrafast and broadband dynamics, low-density species and states, and nonlinear effects, great efforts have been made to commission or upgrade X-ray sources to deliver higher and higher pulse energies, shorter pulse durations, and high repetition rates [9,10]. X-ray sources have significantly improved thanks to the operation of X-ray free-electron laser (FEL) and X-ray high harmonic generations (HHGs), which extend the time resolution of X-ray spectroscopic techniques for the investigation of the electronic structures of materials and to probe their dynamics upon controlled excitation. Nowadays, they also allow for the analysis of ultrafast electronic and structural dynamics in different materials excited by X-ray pulses at the carbon K-edge.

Novel X-ray FEL sources provide highly bright, coherent, wavelength-tunable photon pulses in the femtosecond (fs) domain [11], and seeded FELs provide soft X-ray beams showing laser-like high-order coherence [12]. For instance, with a peak spectral brilliance in the range of  $10^{29}$  to  $10^{34}$  (photon/s.mm<sup>2</sup> m rad<sup>2</sup> 0.1% bandwidth) and a repetition rate from 10 Hz to 100 kHz, soft X-ray FEL allows for high-resolution X-ray experiments and the observation of strong non-linear behaviors. Alternatively, HHG sources offer a full time-spatial coherent femtoseconds and sub-femtoseconds pulse in a very broad X-ray spectral range ( $>300$  eV). Many HHG sources exhibit similar repetition rates and/or shorter pulses suitable for observing single-shot absorption spectra and simultaneous probing of multiple components. These experiments may support the time-resolved reconstruction of many molecular dynamics giving information on different photochemical pathways [13]. The energy tunability of FELs allows excitation-energy-sensitive methods, e.g., spectroscopic techniques and advanced diffraction methods. Moreover, coherence enables X-ray imaging [14] and correlation spectroscopy techniques [15]. Ultrashort pulsed configurations allow for in situ and time-resolved experiments. Finally, further developments are also expected in the future due to the possibility of controlling the beam polarization in such sources.

In this review, we summarize the results achieved by some pioneering experiments near the C K-edge performed with FELs and HHG sources, emphasizing their unique characteristics. Different time-resolved pump-probe spectroscopies will be presented, such as X-ray absorption spectroscopy, photoelectron spectroscopy, and non-linear spectroscopy. These techniques, taking advantage of the unique combination of brilliance, high energy spectral resolution, coherence, femtoseconds pulse duration, and energy and polarization tunability, enable us to investigate the time-resolved evolution of various chemical bonds in catalytic reactions [16] and charge and energy conversion processes, surface plasmon-induced effects in nanostructures [17,18], the fundamental properties of amorphous materials such as glass [19,20], and the dynamics of molecules going through conical intersections.

In Section 2, we present three different experiments performed with FELs at the C K-edge, i.e., time-resolved X-ray absorption spectroscopy (Section 2.1), non-linear spectroscopy (Section 2.2), and photoelectron spectroscopy (Section 2.3), the methods of which have been applied to investigate catalytic reactions, non-linear effects, and the electronic structure dynamics of photo-excited chiral molecules, respectively. Finally, in Section 3, we briefly summarize the results of two recent transient X-ray spectroscopy studies performed with HHG sources at the C K-edge, investigating ultrafast dynamics (Section 3.1) and broad-

band dissociation processes (Section 3.2) in organic molecules near conical intersections. Perspectives are briefly outlined at the end of this review.

## 2. Carbon K-Edge Studies Using FELs

### 2.1. Probing Catalysis in Real Time: Observation of Transient Precursor States

In heterogeneous catalysis, systems such as small gas molecules on a metal surface, reactants adsorbed on surfaces are converted to products, which are eventually desorbed via various intermediates. The chemical bond-breaking reaction, which triggers the desorption of chemisorbed gas molecules and/or their fragmented segments from the surface, is one of the most interesting and complex processes. To achieve a complete understanding of these surface chemical processes, a collection of detailed information on the different steps occurring during the formation and breaking of surface chemical bonds is mandatory [21].

A reference example is represented by the investigation of the transient dynamics of CO interaction with the Ru (0001) transition metal surface. Long-term investigations into the surface-adsorbed CO interaction with Ru (0001) have revealed frustrated rotational motion of CO molecules, which leads to desorption into the gas phase. However, prior to their desorption, an intermediate state of weakly bonded CO occurs, referred to as a precursor state, with a short residence time and a low population of the species. Precursor states support the adsorbed molecules to recover rotational and translational energies before completely breaking the adsorption bond at the surface and entering the gas phase [8,22–24]. Ultrafast pump-probe techniques using soft X-ray FELs could probe the dynamics of molecule desorption by promoting the minimum required population of molecules in transient states suitable for their detection within short timescales. The hot electron and its phonon-mediated excitation of the chemisorbed CO molecules are induced by a synchronized femtosecond optical laser pulse excitation of the Ru (0001) substrate.

During the desorption process, the element-specific time evolution of occupied and unoccupied valence electronic states around adsorbed CO molecules on the Ru(0001) surface could be monitored at the O K-edge using both X-ray emission spectroscopy (XES) and X-ray absorption spectroscopy (XAS) [8]. This experiment, performed using the surface science end station (SSE) at the soft X-ray hutch (SXR) at SLAC using the National Accelerator Laboratory's Linac Coherent Light Source (LCLS), identified both the presence of the precursor state and a translational motion of the CO molecule parallel to the surface [24]. This motion was detected prior to the emergence of the precursor state, showing that time-resolved experiments are an excellent method for detecting short-lived surface species. However, the vibrational broadening of the O K-edge resonance absorption peak in the XAS spectrum, due to multiple excited states that become occupied after the generation of the O1s core-hole, limits the analysis of important aspects of the time evolution of precursor states.

Because of the reduced vibrational broadening, XAS experiments were performed at the C K-edge, looking at the  $1s \rightarrow \pi^*$  resonance, at the FEL DIPROI beamline of the FERMI facility (Trieste, Italy). This experiment provided details on the time evolution of the desorption precursor state. Following the core-hole generation, the excitation at the C K-edge generated sharp spectral features in comparison to those of O [25]. In this experiment, an ultrafast laser pulse, with a duration of 100 fs ( $\leq$  timescale of molecular motions) set at the central wavelength of 400 nm and with a pulse energy of 150  $\mu$ J delivered to the sample to optically pump the chemical reactions. The excited states were probed by soft X-ray pulses shorter than 50 fs at 287 eV (near the C K-edge of chemisorbed CO) at 10 Hz repetition rate. The probe beam was synchronized to the pump with a shot-to-shot temporal jitter of less than 6 fs. The XAS spectroscopy has been used to investigate changes in the molecular orientation using optical pulsed laser excitations with the pump polarization normal to the surface combined with the variable probe polarization (the FEL) tuned from horizontal to vertical, i.e., in-plane and out-of-plane. The temporal dynamics were explored by changing the pump to probe delay from  $-2$  to 150 ps. Spectra were collected by tuning the incident X-ray energy by the standard procedure, i.e., tuning the

seed laser wavelength and the resonance conditions of the undulators. The FERMI FEL spectral bandwidth is 0.3 eV, a value limiting the resolution of any precursor-related peak.

Figure 1 shows pump probe XAS spectra and its layout, clarifying how results could allow us to draw a picture of fast chemical reactions occurring during the desorption of the chemisorbed CO on the Ru surface. The entire process can be summarized as follows: The intensity changes between in-plane and out-of-plane X-ray absorption spectra together with a redshift ( $\sim 0.08$  eV) of the peak positions confirm the occurrence of rotationally and translationally excited chemisorbed CO molecules upon absorption of the photons of the pump laser and the generation of hot electrons at the surface within 100 fs. The rotating molecules move during the first picosecond time domain, from the on-top site towards the bridge or the hollow site, characterized by higher coordination and different potential energy surfaces. Later, the hot electrons gradually heat up the phonon system within the metal crystal triggering coupled electron-phonon modes to excite chemisorbed CO molecules into precursor states within a few picoseconds. In the precursor state, CO molecules rotate isotropically and freely interact with the surface for several picoseconds before desorption or re-adsorption occurs. Polarization-dependent XAS measurements provided further information on ultrafast reorientation effects and confirmed that chemisorption and precursor states are separated by an entropy barrier, as shown in Figure 1b,c. Some excited molecules are trapped before crossing the barriers, creating new adsorption states. Actually, thanks to the sharp resonance peak at the C K-edge, this additional absorption resonance was clearly resolved.

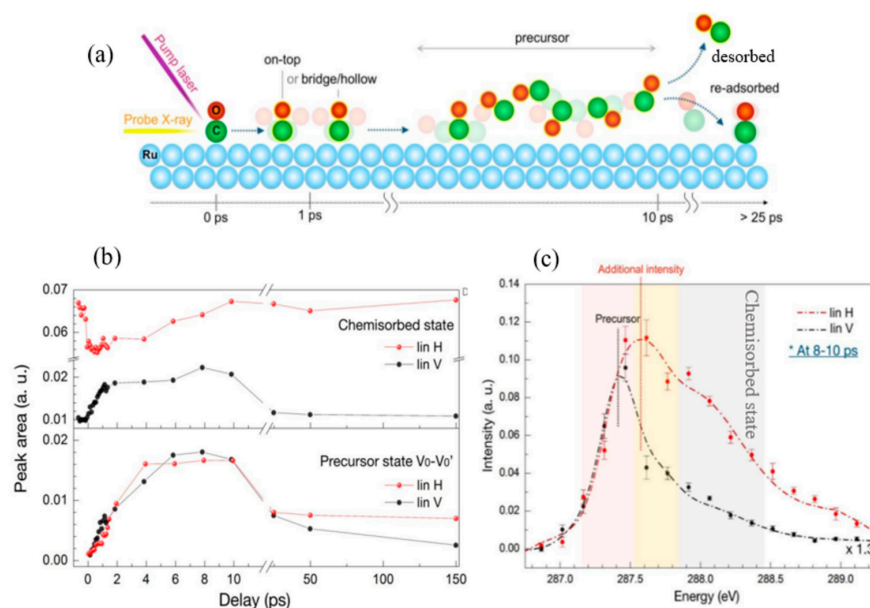


**Figure 1.** (a) Dynamics of optically excited CO chemisorbed on Ru (0001) due to optical laser irradiation, CO molecules rotate and shift toward higher coordinated sites from on-top sites. After converting into the precursor state, CO molecules rotate isotropically, bonding the surface for several picoseconds before desorption or re-adsorption by the surface. (b) Time-dependent evolution of the integrated intensity of the characteristic states estimated from horizontal (H) and vertical (V) linear polarized X-ray absorption spectra. (c) Comparison between the H and V spectra at 8–10 ps delay, which clarifies that there must be an additional state between the chemisorbed and precursor states. (Reused from [25] with the permission of PCCP Publishing).

The prospect of exploring surface chemistry and catalysis using X-ray lasers at the C K-edge can be enhanced by further development of coherent sources. Given the narrow linewidth of the CO gas's C K-edge in the X-ray absorption spectrum ( $<0.18$  eV), the higher resolution of the FEL probe ensures better resolved spectral characteristics. For this class of experiments, a high repetition rate from the source is advantageous to compensate for the low cross-section of the effects that is not easily compensated even at the high

intensity of X-ray FEL pulses. The FEL probe can also be combined with an intense THz pump to provide information on selectively triggered CO oxidation on Ru (0001). It has been demonstrated that the ultrashort intense electric field of the THz pulse can orient only the CO oxidation producing CO<sub>2</sub> as compared to optical excitations that induce both CO desorption and CO oxidation with the preference for the desorption pathway due to heating [3,26]. Actually, an intense THz pump combined with a powerful FEL probe represents a unique tool to investigate the feasibility to tune chemical processes.

## 2.2. Intense FEL-Induced Nonlinear Effects

An intense radiation–matter interaction is referred to as a “non-linear response” when it modifies a material’s optical properties in such a way that its optical response is nonlinearly dependent on the intensity of the incident field [27]. Nonlinear phenomena, including second harmonic generation, two-photon excitations, and saturable absorptions, have been extensively studied at optical and UV wavelengths. Extending non-linear studies to shorter wavelengths offers a unique chemical- and element-specific probe. However, the lack of extremely bright X-ray sources with a high degree of spatial and temporal coherence has hindered the investigation of non-linear effects in the X-ray domain. Following the availability of X-ray FELs delivering extremely bright, ultrashort and highly coherent pulses, these studies are now possible.

The observation of nonlinear effects in graphite at the C K-edge was achieved at the EIS-TIMEX end station at the FERMI FEL-2 facility in different experiments [28–30]. Graphite samples 100–700 nm thick were exposed to a tunable soft X-ray seeded FEL pulse 25 fs (FWHM) long and with a spot size of 350 μm<sup>2</sup> at different photon energies: 260.5 eV (non-resonant), 284.18 eV or 285.7 eV (on-resonance), and 307 eV and 309.2 eV (above resonance). The transmitted beam was detected by a CCD camera after attenuation with aluminum or nickel filters, spectrally and spatially separating the beam going through the spectrometer. The measured absorption spectrum of graphite in a linear regime and the experimental setup are shown in Figure 2a,b, respectively.

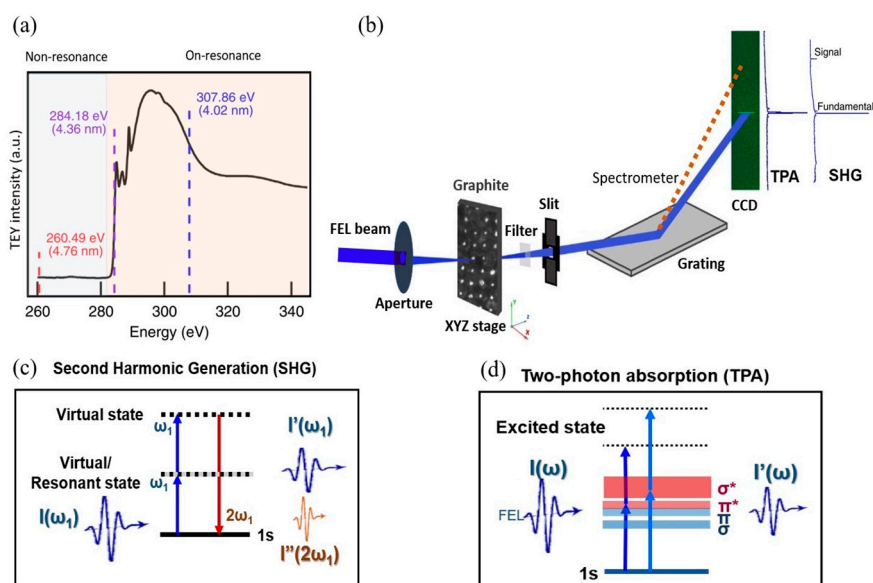


**Figure 2.** (a) Total electron yield (TEY) X-ray absorption spectrum of a 500 nm graphite sample in the linear regime. Nonlinear effects in X-ray measurements were observed at the three discrete photon energies shown with the dashed lines. The non-resonant and resonant regions are shaded in blue and orange showing below and above the C K-edge, respectively. (b) The experiment layout. (Reproduced from [28] with the permission of ElseVier Publishing.) Schematic view of the dominant processes of (c) second harmonic generation (SHG) and (d) two-photon absorption.  $I(\omega)$  and  $I'(\omega)$  represent the intensity of the incoming and transmitted beams,  $\pi$  and  $\sigma$  are bonding orbitals whereas  $\pi^*$  and  $\sigma^*$  are antibonding orbitals, respectively [28–30].

### 2.2.1. Second Harmonic Generation by Graphite

The second harmonic generation (SHG) process in infrared, visible to ultraviolet photon energy ranges is generated by the interaction of an intense coherent beam with a medium characterized by a broken inversion symmetry, such as surfaces and interfaces, that generates a doubled frequency field. According to the resonance effect, the perturbation theory points out that the SHG signal increases by tuning the photon energy of the ultrashort soft X-ray pulse to the binding energy of the absorption edge of the material under investigation [11,29]. The pulse energy ( $\sim 1\text{--}5\ \mu\text{J}$ ) dependence of the soft X-ray SHG below and above the C K-edge for graphite with different thicknesses shows the resonance enhancement of the second harmonic signal. According to [29], the SHG signal at soft X-ray wavelengths should be an interface-specific probe.

The phenomenon is evident when the required pulse energy onset is one order of magnitude lower than that of the off-resonant incident pulse. It is also independent of the thickness of the sample, confirming the surface sensitivity of the process. The resonance enhancement property at the interface supports elemental and chemical-sensitive spectroscopic techniques with a broad potential for applications in many scientific areas. SHG spectroscopy with a soft X-ray FEL may provide element-selective information from a multi-element material or from non-homogeneous structures [31], in ultrafast dynamics at heterojunction systems, interfaces of 2D materials or buried interfaces in a layered sample. The ability to preserve coherence allows this approach to be combined with lensless coherent imaging techniques such as atomic electron tomography with aberration-free resolution [32]. In addition, as significantly smaller fields are required for soft X-ray SHG, almost damage-free measurements can be performed by exploiting the higher repetition rate of FELs combined with large and efficient 2D detection systems.

### 2.2.2. Two-Photon Absorption by Graphite

Two-photon absorption (TPA) is a fundamental third-order non-linear optical process in which two photons are absorbed simultaneously. TPA effects are only observed on-resonance, i.e., just below the carbon  $1s \rightarrow \pi^*$  transition in graphite, in X-ray-intensity-dependent transmission measurements for different sample thicknesses, i.e., by gradually decreasing the transmission. The transmission above and below the resonance is constant in the experiment's intensity range ( $< 10^{30}\ \text{photon cm}^{-2}\ \text{s}^{-1}$ ), and the source behaves as a nonlinear absorption-free probe at off-resonance energies near the K-edge. It is mandatory to account for this effect when analyzing time-resolved soft X-ray absorption spectroscopy with an FEL [28]. The results show that TPA is a bulk probe, possible in centrosymmetric systems, at soft X-ray energies, is element selective and, similar to SHG, is significantly enhanced for energies of the incident photon near the absorption edge of an atom of the material. It is also worth mentioning that the interpretation of TPA's strength can be hampered by FEL's energy fluctuations [28,30].

### 2.2.3. Saturable Absorption by Graphite

Soft X-ray-induced transparency or saturable absorption (SA) using FEL radiation is another phenomenon that has recently been observed at the C K-edge, which is being competitive with TPA and depends on the pulse intensity. Experiments at photon energies of 285.7 and 309.2 eV were performed on an 80 nm thick graphite sample to match the  $1s \rightarrow \pi^*$  and  $1s \rightarrow \sigma^*$  transitions of carbon. Transmission measurements vs. intensity of the X-ray pulses pointed out sub-linear and super-linear trends for transitions to  $\pi^*$  and  $\sigma^*$  states, which refer to TPA and SA non-linear effects, respectively. Observations and theoretical calculations both suggest that the depletion of the core by an intense FEL pulse drives the SA effect, depending on the rate of the Auger decay, which is  $\sim 7\ \text{fs}$  in graphite. At higher intensities, TPA dominates at both photon energies with a different onset [30]. These results are useful to better understand soft X-ray absorption and scattering data at high intensities.

### 2.3. The Electronic Structure of Photo-Excited Chiral Molecules

Chiral molecules, such as chiral amino acids, are characterized by broken mirror symmetry, in other words they cannot be superimposed on their mirror image. Despite having identical chemical structure, optical isomers or enantiomers exhibit distinct chemical characteristics when they interact with other chiral systems, such as circularly polarized light or chiral reactants. Understanding and controlling the chiral activity of photoexcited states can be accomplished by probing the dynamics of these molecules. Photoelectron circular dichroism (PECD), which is the asymmetric ionization of a randomly oriented enantiomeric sample using circularly polarized radiation, is a promising technique for investigating the chirality of molecules in the gas phase. Here, we must introduce the chiral asymmetry factor, which is defined as the normalized difference between the angular distribution of left- and right-handed circularly polarized light.

Recent time-resolved PECD investigations of valence-shell to the Rydberg state excitations showed that the method may probe ultrafast intramolecular relaxation providing unique information on alignment, vibrational relaxation, and electronic conversion [33]. However, the source of the asymmetries was not resolved, i.e., it was not clear if it is induced by the initial orbital or by the chirality of the surrounding effective potential. To recognize the origin of an asymmetry, an ultrashort, high-brilliance circularly polarized soft X-ray source, such as an FEL directly inducing a core-level ionization, may allow for a potentially localized and chemically sensitive in situ probe of the photoelectron scattering by a chiral molecular potential.

Experimental data confirmed that a soft X-ray FEL source is very effective in time-resolved PECD for studying dissociating chiral cations [34] and for time-resolved photoelectron spectroscopy (XPS) applied to site-specific analysis suitable for distinguishing between the contributions of different atoms of the same chemical element that are simultaneously probed [35]. Following these promising results, Faccialà et al. investigated at the C K-edge the chirality of fenchone, a prototypical organic molecule, using both time-resolved XPS and PECD [36]. The experiment was carried out at the FERMI-FEL, currently the only facility that delivers high-temporal coherent and circular polarized pulses in this energy domain. The authors used seeded FEL pulses with circular polarization at 300 eV, a duration of ~15 fs and a repetition rate of 10 Hz synchronized with the pump to the interaction region in a quasi-collinear geometry (angle ~0.6°). Figure 3 displays the layout of the experiment apparatus and the investigated molecule.

Core-level photoelectron spectroscopy (PES) and PECD C K-edge ionization experiments of the ground state, i.e., without pump, of fenchone using FEL radiation identified that the binding energy of the weak peak of the carbonyl 1s ( $C_1$ ) upshifted with respect to the other carbon sites with an asymmetry up to 20%. The TR-PES results and corresponding calculations are presented in Figure 3a–e, where the chiral asymmetry factor ( $\sigma_0$ ) is defined as the normalized difference between the left- and right-handed CPL angular distributions. Time-resolved experiments using PES and PECD, looking at the excited state, were carried out at different pump-probe delays in the range 200–1000 fs. A linearly polarized UV laser at 400 nm with a pulse duration of 75 fs was used to excite molecules from a localized orbital to a diffuse molecular 3s Rydberg state through a two-photon absorption process. The excitation not only triggers the ultrafast relaxation dynamics, but also redistributes the valence electron density, inducing a short-term chemical shift of the core electron binding energies that enhances the site-specificity.

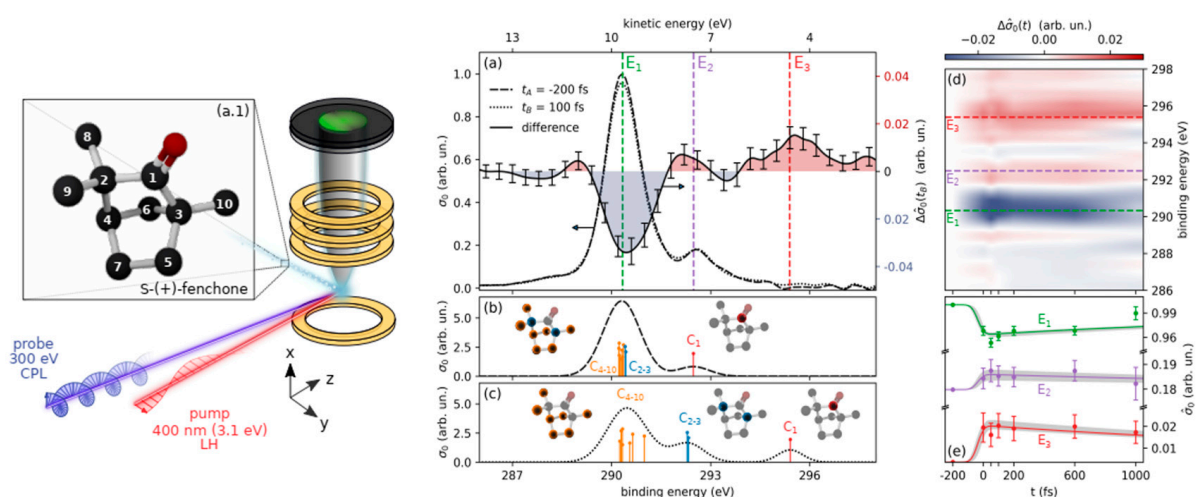


**Figure 3.** (Left): Experimental layout. The linear horizontal (LH) polarization visible pump and the circularly polarized X-ray probe, noted by CPL in the schema, are focused quasi-collinearly in the molecular beam of S-(+)-fenchone optical isomers. (Left (a.1)): A 3D model of the S-(+)-fenchone with only carbon (labeled from 1 to 10) and oxygen atoms displayed in black and red, respectively, and hydrogen atoms were omitted for the sake of simplicity. (Right): (a–e) experimental and calculation results of TR-PES; (a) PES at  $t_A = -200$  fs (dashed line), and  $t_B = 100$  fs (dotted line), difference  $\Delta\hat{\sigma}(t_B) = \hat{\sigma}_0(t_B) - \hat{\sigma}_0(t_A)$  of the sliding averaged PES  $\hat{\sigma}_0$  (solid line and  $1\sigma$  error-bars). (d)  $\Delta\hat{\sigma}(t)$  for all the measured delays  $t$ . (a,d) The energies  $E_1$ ,  $E_2$  and  $E_3$  are indicated by dashed green, violet and red lines, respectively. (e)  $\hat{\sigma}_0(t)$  for  $E_1$ ,  $E_2$  and  $E_3$  is indicated by green, violet and red dots, respectively, along with the  $1\sigma$  error-bars. A single exponential of 3.3 ps decay time, corresponding to the measured lifetime of the 3s Rydberg state is shown with solid lines. (b,c) Calculated binding energies for the ground state (b) and excited 3s Rydberg state (c), indicated by red ( $C_1$ ), blue ( $C_2$ ,  $C_3$ ) and orange (from  $C_4$  to  $C_{10}$ ) dots and vertical lines, where the vertical offset is intended for the sake of clarity only. Theoretical PES in (b,c) are shown with dashed and dotted lines, respectively. (Reused with permission [36]. Copyright @ Creative Commons Attribution license (CC BY 4.0) (2022), by Michele DeVetta).

Calculations confirmed the wide separation among carbon at  $C_1$ ,  $C_2$ , and  $C_3$  sites in the time-resolved PES spectra (see Figure 3c). In comparison, time-resolved PECD experiments enabled the observation of the chiral electronic structure and of the relaxation dynamics following the excitation. The chiral asymmetry and the binding energy of the 1s carbon states of this molecule in the excited 3s Rydberg state change due to the different local chiral surroundings of each excited carbon atom. Experimental observations and calculations demonstrated that the asymmetry factor at the shifted binding energy of the  $C_1$  atom originates from the ground state and it is further up-shifted, whereas the positive contribution of  $C_{2-3}$  originates from the excited 3s Rydberg state and resolve the  $C_{1-3}$  ( $C_2$ - $C_1$ (=O)- $C_3$ ) contribution by the upshift. Time-resolved PECD measurements performed in the excited states allowed us to study the local chirality of the electronic environment surrounding these sites, blended by the contributions of all other sites present in the ground state. These findings contribute to TR-chiral XPS, a novel enantio-specific, site- and chemical-specific spectroscopic method suitable to investigate chiral molecules.

However, in these experiments, the time-resolved PECD signal cannot be resolved in the whole energy range of interest because of the weak response associated with the low excitation efficiency ( $\sim 12.5\%$ ). Using a high flux and a short excitation pulse, the excitation efficiency could be enhanced. A high-repetition-rate FEL probe would provide a more intense photon flux to the sample, maximizing the chiral response and allowing for PECD measurements. Finally, it must be underlined that faster responses of chiral vibrational dynamics, up to 100 fs, need to be explored.

### 3. Carbon K-Edge Studies with HHG Sources

#### 3.1. Ultrafast Electronic and Structural Dynamics of Organic Molecules at Conical Intersections

In quantum mechanics, potential energy surfaces for the motion of atomic nuclei are defined by the interplay of molecular energy vs. molecular geometry. The underlying potential energy landscape determines the structural dynamics of any photoexcited molecule. Both electronic and nuclear degrees of freedom are addressed in the separated electronic and nuclear coordinates, which refer to the so-called Born–Oppenheimer approximation, where the dimension of the potential energy surface equals the nuclear degree of freedom. In the adiabatic approximation the time-dependent Schrödinger equation is solved for electrons at given fixed nuclear positions and then electronic energies as a function of the fixed nuclear coordinates are obtained. When two potential energy surfaces collide, degeneracy regions in the electronic potential energy surfaces occur. The latter known as conical intersections (CIs) are regions where electrons and nuclei become coupled and evolve on comparable timescales so that the Born–Oppenheimer (adiabatic) approximation breaks down. Because of the presence of CIs in the electronic energy landscape, ultrafast non-radiative relaxation pathways may occur through electronic state transitions involving dynamical changes in the molecular geometry [37,38].

The development of novel HHG and FEL sources with significant time and spatial resolutions recently enabled direct, real-time tracking of the coupled electron-nuclear dynamics in photoexcited molecules. Moreover, the most recent advances in attosecond transient absorption spectroscopy (ATAS) using novel sources have made it possible to study the coupled electro-nuclei dynamics close to CIs with extreme time resolutions. The extension of the ATAS method's to C K-edge provides a chance to access the fastest chemical reactions in various organic compounds [39–41]. Recently, ATAS has been applied to study the fast electronic relaxation dynamics of a prototypical organic chromophore, the ethylene ( $C_2H_4$ ), within a time frame shorter than the single vibrational period [39]. The experimental apparatus and the ATAS results obtained in this experiment are presented in Figure 4a–e. The layout of the experiment shown in Figure 4a includes a laser, which is used to generate pulses with an average energy of 2.5 mJ centered at 1.8  $\mu m$ , compressed down to 10 fs i.e., the time resolution of the experiment. Pulses were split into two components; one served as the pump, while the other was used to generate the soft X-ray probe going through a helium-filled gas target for the high-order harmonic generation (HHG). Both pump and probe pulses propagated co-linearly and were focused on the sample with different delays. The transient absorption spectra were collected by measuring the X-ray supercontinuum transmission through the spectrometer (grating/X-ray CCD in the figure).

The pump-off experiment demonstrated that the  $C\ 1s \rightarrow \pi^*$  transition dominates the soft X-ray absorption of the neutral  $C_2H_4$  in its electronic ground state ( $S_0$ ), followed by the onset of the broad continuum absorption (Figure 4b). Upon excitation, a shift of the  $1s \rightarrow \pi^*$  transition to higher energies together with the appearance of an absorption peak corresponding to the  $1s \rightarrow \pi$  transition into a single occupied molecular orbital is also observed. Changes in the optical density in the pump-on spectrum measured are observed looking at the logarithmic ratio of pump-on-to-pump-off intensity (Figure 4c). The transient spectra (Figure 4d) also revealed periodic oscillations of the  $1s \rightarrow \pi$  and  $1s \rightarrow \pi^*$  features at 281 and 286 eV, respectively, together with a short-lived transient centered at 284 eV (dashed red box in Figure 4d). A comparison with simulations revealed that the two first features can be assigned to  $D_0$  states, while the latter can be assigned to the  $D_1$  state. A fast electronic relaxation occurs in  $\sim 6.8$  fs through the conical intersection, which is accessed by stretching the C=C bond as mapped by the ATAS method. The relaxation time of  $D_1 \rightarrow D_0$  is shorter than the single C=C stretching vibrational period and the energy differences between  $D_1$  and  $D_0$  results from the different occupations of the two orbitals lying below the  $\pi^*$  orbital (see Figure 4e). The electronic and the structural relaxations of the  $D_0$  state are probed by the periodic oscillations of  $1s \rightarrow \pi$  and  $1s \rightarrow \pi^*$  transitions and opposite energy shifts. Data confirm the ability of the transient soft X-ray absorption spectroscopy in mapping structural dynamics by looking at the spectral position of X-ray

absorption structures. This approach represents an element-sensitive method for tracking ultrafast electronic and structural dynamics of simple molecules.

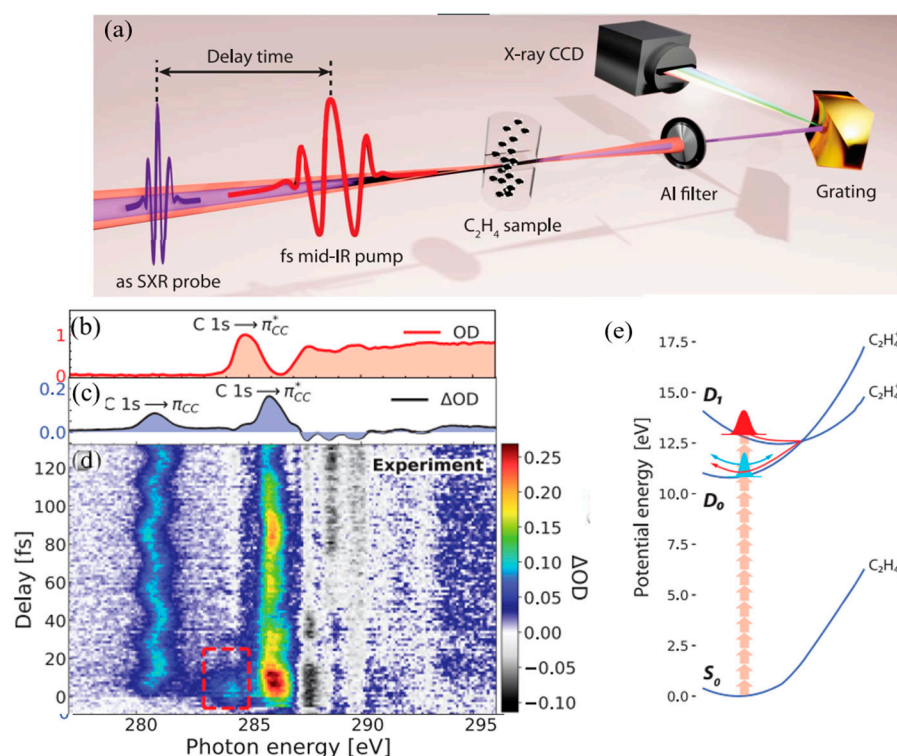


**Figure 4.** (a) Experimental setup. CCD, charge-coupled device. (b) The optical density (OD) of the unexcited target and (c) it changes under the action of the pump pulse ( $\Delta OD$ ). (d) The experimental  $\Delta OD$  as a function of pump -probe delay. The dashed red box indicates the signal assigned to the  $D_1$  state of  $C_2H_4^+$ . (e) Scheme of the conical intersection between the  $D_1$  and  $D_0$  states of  $C_2H_4^+$  mediating the electronic relaxation. (Reused from [39], Copyright©2021, American Association for the Advancement of Science).

This investigation visualizes electronic relaxation faster than the shortest vibrational periods and points out the fundamental role of sub-femtosecond spectroscopy for a better understanding of excited-state dynamics in molecules through the clear separation of electronic and structural dynamics. At the C K-edge, attosecond spectroscopy is going to provide a wide range of opportunities to study a broad class of organic molecules on the useful timescale, for instance, to reconstruct isomerization reactions [42,43]. It may also enable studies of solvated molecules giving access to solvation effects on the timescales of conical intersection dynamics [44] and electronic decoherence due to the electronic coherent control over CI dynamics.

### 3.2. Time-Resolved Photodissociation Reactions of Molecular Cations

The HHG technique has been used to create a tabletop soft X-ray supercontinuum within the range of 150 to 350 eV. In this domain, we may look at unexplored photochemical reactions in the lowest electronic states of  $CF_4^+$  and  $SF_6^+$  molecular cations in the gas phase [45]. By considering the alteration of the dipole selection rules by molecular symmetry and the sensitivity of time-resolved X-ray absorption near edge structure (XANES) spectroscopy to chemical shifts and symmetry lowering, the splitting of the originally triply degenerated orbitals of  $CF_4$  and  $SF_6$  into doubly degenerated or nondegenerate orbitals was observed. Moreover, since in this experiment, soft X-ray pulses probe the spatial arrangement of molecules' unoccupied valence orbitals, modifications occurring during photochemical dissociation processes that transform the molecule from neutral to cation can be also recognized. To generate high harmonics, a long-wavelength beam of 1800 nm

with 2.5 mJ of energy at 1 kHz is traveling through a high-pressure neon gas cell. The generated X-ray radiation was then directed to the sample gas cell together with ultrashort 800 nm pulses focused on the sample surface. The latter pulses, having a peak intensity of  $5 \times 10^{14}$  W/cm<sup>2</sup>, acted as pump.

The transmitted soft X-ray radiation passing through a grating produced an energy spectrum that was collected using a microchannel plate (MCP) detector. Data for the CF<sub>4</sub> are presented in Figure 5a,b. The broadband spectrum through the CF<sub>4</sub> gas (Figure 5a) is characterized by an absorption peak at 298 eV, which could be assigned to transitions  $1s \rightarrow 5t_2$  and  $6t_2$  to unoccupied triply degenerate orbitals,  $\sigma^*$ . Upon the ionization of the CF<sub>4</sub> by the pump pulse, the molecule dissociates spontaneously into CF<sub>3</sub><sup>+</sup> and F as it has been presented schematically in the Figure 5c. The evolution of the molecules during the dissociation process was tracked by time resolved X-ray absorption spectroscopy with different pump-probe time delays (Figure 5b). An increase in the absorbance, a red shift of the maximum and a progressive splitting into multiple bands were observed. Such changes in the absorption spectrum are the signature of the symmetry decrease driven by the photodissociation from the initially tetrahedral CF<sub>4</sub><sup>+</sup> to the trigonal planar CF<sub>3</sub><sup>+</sup> molecule and the energy decrease due to the Jahn–Teller effect [46].

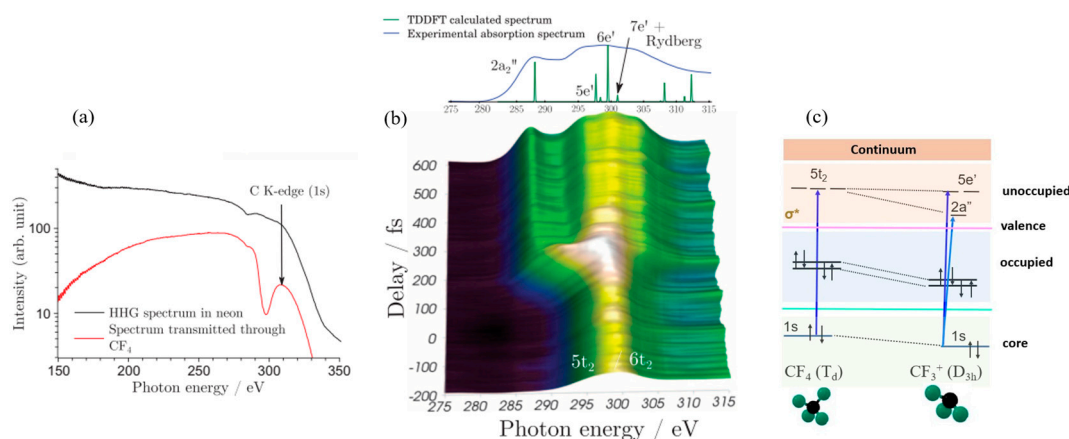


**Figure 5.** (a) High-harmonic spectrum at the carbon K-edge and transmitted spectrum through CF<sub>4</sub> gas. (b) Transient absorption spectroscopy at the C K-edge. Absorbance  $A(t) = \ln[I_0/I(t)]$  as a function of the NIR pump–X-ray probe time delay. Negative time delays correspond to unpumped condition. The intensity axis, as well as the color scale, are linear. The calculated stick spectrum in the upper panel is the comparison between experiments and calculation. (c) Orbital diagram illustrating selected transitions. (Reused from [45], Copyright©2017, American Association for the Advancement of Science).

In addition to the two cases quoted before, there are several other examples where theoretically foreseen phenomena can be investigated using these novel X-ray sources. For example, time-resolved X-ray absorption spectroscopy at the C K-edge can visualize the vibronic dynamics of the photoexcited ICN dissociation processes moving through the gas phase CI when X-ray ultrashort and intense pulses are used as a probe. According to simulations, the broadband I-CN bond breaks and the vibronic behavior of molecular fragments occurs on a timescale of less than 100 fs [47]. The process is visible in experiments with HHG sources with a spectral resolution up to 1.2 eV and a time resolution of a few fs [39].

The position of conical intersections, where non-adiabatic effects control transition probabilities among different electronic states, is crucial for light-driven molecular reactions. The results and timing of nonadiabatic molecular dynamics are clear signatures of relaxation processes. Recent theoretical and experimental findings demonstrate that the position of CI can be affected by strong hydrogen bonds in protein-related non-aromatic amino acids, causing photoexcited molecules to radiatively relax [48]. We are convinced that in the near future the mechanisms occurring near the C K-edge in photoexcited molecules in the CI

domain will be observed and recognized using time-resolved soft X-ray spectroscopies with FEL or HHG sources.

#### 4. Conclusions and Outlook

Soft X-ray spectroscopies using modern pulsed sources represent powerful tools to exploit challenging scientific and technological phenomena. Bond-breaking, structural isomerization, polarization-dependent phenomena, non-adiabatic dynamics of photoexcited molecular systems, and non-linear effects, which are briefly summarized in this short review, are just some of the ultrafast chemical reactions that could be probed by soft-X-ray FELs and HHG sources at the C K-edge. The advancements in the pulse duration, spectral resolution, spectral control, and spot size of these novel sources operating in the water window and below the C K-edge will be strategic for investigating these effects accurately and comprehensively. An FEL pump can offer an elemental selective excitation combined with the HHG source probe, which can provide more information in comparison with the experiments based on the HHG probe that uses an optical pump. Recent investigations demonstrate that FEL pulses of a few femtoseconds (1–2 fs) duration is achieved through the superradiant cascade approach in seeded FELs [49,50]. Moreover, novel experimental techniques have been proposed for monitoring ultrafast dynamics and will be tested over the coming years at different facilities [38,47,51–55].

Keefer et al. recently suggested experimental techniques looking at the transient redistribution of ultrafast electronic coherence in the attosecond Raman signal (TRUECARS). This approach could be used to monitor CIs dynamics of the uracil RNA-nucleobase [38,51]. Different features of a soft X-ray FEL, e.g., high energy, broader frequency tunability and the capability to generate attosecond pulses could be used to explore the vibronic coherence, a mechanism that appears when molecules pass through conical intersections. Upon a laser-stimulated Raman process, phase-controlled hybrid broadband/narrowband, attosecond and femtosecond X-ray pulses can be used to probe this non-adiabatic process.

HHG sources generating single-shot absorption spectra allowing living-cell imaging with a femtosecond time resolution are also capable of generating attosecond pulses with a high intensity [52]. Time-resolved photoelectron spectroscopy with attosecond pulse trains could be used to resolve the electronic coherence in the time domain as well as the electronic states involved in the CIs in the energy domain with an acceptable energy resolution [53]. In this configuration, an FEL source is supposed to be competitive with an HHG source [44].

The approach to polarized resonant soft X-ray scattering (P-RSoXS) is similar to that of small-angle X-ray scattering (SAXS). This new method that selects individual elements and specific bonds may return spatial and spectral information about orientation features in amorphous soft materials too. The sensitivity to soft X-ray transition dipoles provides the basis for a quantitative characterization of the molecular orientation on the nanoscale, which can offer a strategic tool for the investigation of polymer nanocomposites and membranes as well as more complex chemically heterogeneous systems such as long polymeric chains [47,54].

A wide variety of theoretically simulated ultrafast dynamics, e.g., vibronic dynamics [48,56,57] could be explored with these next-generation soft-X-ray sources combined with innovative experimental methods, detectors, and computational capabilities. A high-repetition-rate FEL source combined with more efficient detection systems will be extremely useful to perform damage-free measurements of non-linear effects.

With limited cross-sections and/or low-populated species, high repetition-rate FEL sources will be very attractive. In addition, the spectral resolution enhancement will give more insight into spectral characteristics. One of the next-generation soft X-ray FEL sources is EuPRAXIA@SPARC\_LAB, a facility under development in Italy at the Laboratori Nazionali di Frascati of the INFN. This radiation facility is an essential component of the European EuPRAXIA project that intends to establish a plasma-accelerated FEL facility promising size and cost savings [58–60]. Two beamlines are planned: a seeded FEL in the

VUV range 25–7 eV (50–180 nm) oriented to the study of atomic and molecular systems named ARIA [61], and an SASE SXFEL operating in the water window 310–200-eV (4–6 nm) named AQUA [62]. Their construction will expand FEL research and technology to new concepts and opportunities, also relying on the plasma-based acceleration. The AQUA beamline spectral domain matches the core absorption edge of carbon, and it will be ideal for performing experiments similar to those reviewed in this paper [63].

To enhance beam transfer, manipulation, and detection, innovative, low-loss, and compact optical devices such as beam-splitting off-axis zone plates [64], monochromators [65], and MCP devices can be introduced in soft X-ray beamlines. For example, using MCP devices, X-ray pulses can be delivered to the sample while preserving the source brilliance. In the soft X-ray range, these small-footprint optical devices are particularly efficient and may keep the coherence of the radiation emitted by these sources [66]. MCPs may act as condensing and focusing lenses, and their compact size and short operating distance may also allow one to reduce the overall length of beamlines [67–69].

At the experimental station, a wider variety of materials and larger molecules may be handled by the new sample delivery techniques for substances and materials in the liquid [70] or gas phase [71]. Finally, using the most advanced data collection techniques, such as ghost imaging, we may also improve the resolution while reducing the time of data acquisition and storage for time- and energy-resolved experiments [15,72,73].

**Funding:** This work has been supported by the European Union Horizon 2020 research and innovation program, Grant Agreement No. 653782 (EuPRAXIA).

**Data Availability Statement:** Not applicable.

**Conflicts of Interest:** The authors declare no conflict of interest.

## References

1. Smith, N. Science with Soft X Rays. *Phys. Today* **2001**, *54*, 29–34. [[CrossRef](#)]
2. Wong, L.J.; Kaminer, I. Prospects in x-ray science emerging from quantum optics and nanomaterials. *Appl. Phys. Lett.* **2021**, *119*, 130502. [[CrossRef](#)]
3. Nascimento, D.R.; Zhang, Y.; Bergmann, U.; Govind, N. Near-Edge X-ray Absorption Fine Structure Spectroscopy of Heteroatomic Core-Hole States as a Probe for Nearly Indistinguishable Chemical Environments. *J. Phys. Chem. Lett.* **2020**, *11*, 556–561. [[CrossRef](#)] [[PubMed](#)]
4. Rabe, P.; Kamps, J.J.A.G.; Sutherlin, K.D.; Linyard, J.D.S.; Aller, P.; Pham, C.C.; Makita, H.; Clifton, I.; McDonough, M.A.; Leissing, T.M.; et al. X-ray free-electron laser studies reveal correlated motion during isopenicillin N synthase catalysis. *Sci. Adv.* **2021**, *7*, eabh0250. [[CrossRef](#)] [[PubMed](#)]
5. Rezvani, S.; D’Elia, A.; Macis, S.; Nannarone, S.; Lupi, S.; Schütt, F.; Rasch, F.; Adelung, R.; Lu, B.; Zhang, Z.; et al. Structural anisotropy in three dimensional macroporous graphene: A polarized XANES investigation. *Diam. Relat. Mater.* **2021**, *111*, 108171. [[CrossRef](#)]
6. Di Cicco, A.; Rezvani, S.J.; Nannarone, S. Revisiting the Probing Depths of Soft X-ray Absorption Techniques by Constant Initial State Photoemission Experiments. *Springer Proc. Phys.* **2021**, *220*, 85–97. [[CrossRef](#)]
7. Di Cicco, A.; Polzoni, G.; Gunnella, R.; Trapananti, A.; Minicucci, M.; Rezvani, S.J.; Catone, D.; Di Mario, L.; Cresi, J.S.P.; Turchini, S.; et al. Broadband optical ultrafast reflectivity of Si, Ge and GaAs. *Sci. Rep.* **2020**, *10*, 17363. [[CrossRef](#)]
8. Dell’Angela, M.; Anniyev, T.; Beye, M.; Coffee, R.; Föhlisch, A.; Gladh, J.; Katayama, T.; Kaya, S.; Krupin, O.; LaRue, J.; et al. Real-Time Observation of Surface Bond Breaking with an X-ray Laser. *Science* **2013**, *339*, 1302–1306. [[CrossRef](#)]
9. Matsuda, I.; Kubota, Y. Recent Progress in Spectroscopies Using Soft X-ray Free-electron Lasers. *Chem. Lett.* **2021**, *50*, 1336–1344. [[CrossRef](#)]
10. Rossbach, J.; Schneider, J.R.; Wurth, W. 10 years of pioneering X-ray science at the Free-Electron Laser FLASH at DESY. *Phys. Rep.* **2019**, *808*, 1–74. [[CrossRef](#)]
11. Geloni, G.; Huang, Z.; Pellegrini, C. *X-Ray Free Electron Lasers: Applications in Materials, Chemistry and Biology*; Bergmann, U., Yachandra, J.Y., Eds.; Royal Society of Chemistry: London, UK, 2017; pp. 1–44. [[CrossRef](#)]
12. Gorobtsov, O.Y.; Mercurio, G.; Capotondi, F.; Skopintsev, P.; Lazarev, S.; Zaluzhnyy, I.A.; Danailov, M.B.; Dell’Angela, M.; Manfreda, M.; Pedersoli, E.; et al. Seeded X-ray free-electron laser generating radiation with laser statistical properties. *Nat. Commun.* **2018**, *9*, 8–13. [[CrossRef](#)] [[PubMed](#)]
13. Costantini, R.; Morgante, A.; Angela, M.D. Excitation density in time-resolved water window soft X-ray spectroscopies: Experimental constraints in the detection of excited states. *J. Electron Spectrosc. Relat. Phenom.* **2022**, *254*, 147141. [[CrossRef](#)]

14. Chapman, H.; Barty, A.; Bogan, M.J.; Boutet, S.; Frank, M.; Hau-Riege, S.P.; Marchesini, S.; Woods, B.W.; Bajt, S.; Benner, W.H.; et al. Femtosecond diffractive imaging with a soft-X-ray free-electron laser. *Nat. Phys.* **2006**, *2*, 839–843. [[CrossRef](#)]
15. Li, S.; Driver, T.; Alexander, O.; Cooper, B.; Garratt, D.; Marinelli, A.; Cryan, J.P.; Marangos, J.P. Time-resolved pump-probe spectroscopy with spectral domain ghost imaging. *Faraday Discuss.* **2021**, *228*, 488–501. [[CrossRef](#)] [[PubMed](#)]
16. Ebrahimpour, Z.; Pliekhova, O.; Cabrera, H.; Abdelhamid, M.; Korte, D.; Gadedjisso-Tossou, K.S.; Niemela, J.; Stangar, U.L.; Franko, M. Photodegradation mechanisms of reactive blue 19 dye under UV and simulated solar light irradiation. *Spectrochim. Acta Part A Mol. Biomol. Spectrosc.* **2021**, *252*, 119481. [[CrossRef](#)]
17. Ebrahimpour, Z.; Mansour, N. Plasmonic Near-Field Effect on Visible and Near-Infrared Emissions from Self-Assembled Gold Nanoparticle Films. *Plasmonics* **2018**, *13*, 1335–1342. [[CrossRef](#)]
18. Maoz, B.M.; Chaikin, Y.; Tesler, A.B.; Bar Elli, O.; Fan, Z.; Govorov, A.O.; Markovich, G. Amplification of chiroptical activity of chiral biomolecules by surface plasmons. *Nano Lett.* **2013**, *13*, 1203–1209. [[CrossRef](#)]
19. Shibuya, T.; Takahashi, T.; Sakaue, K.; Dinh, T.-H.; Hara, H.; Higashiguchi, T.; Ishino, M.; Koshiba, Y.; Nishikino, M.; Ogawa, H.; et al. Deep-hole drilling of amorphous silica glass by extreme ultraviolet femtosecond pulses. *Appl. Phys. Lett.* **2018**, *113*, 171902. [[CrossRef](#)]
20. Ahmadi, F.; Ebrahimpour, Z.; Asgari, A. Titania nanoparticles embedded Er<sup>3+</sup>-Sm<sup>3+</sup> co-doped sulfophosphate glass: Judd-Ofelt parameters and spectroscopic properties enhancement. *J. Alloys Compd.* **2020**, *843*, 155982. [[CrossRef](#)]
21. Bergmann, U.; Kern, J.; Schoenlein, R.W.; Wernet, P.; Yachandra, V.K.; Yano, J. Using X-ray free-electron lasers for spectroscopy of molecular catalysts and metalloenzymes. *Nat. Rev. Phys.* **2021**, *3*, 264–282. [[CrossRef](#)]
22. Föhlisch, A.; Nyberg, M.; Hasselström, J.; Karis, O.; Pettersson, L.G.M.; Nilsson, A. How carbon monoxide adsorbs in different sites. *Phys. Rev. Lett.* **2000**, *85*, 3309–3312. [[CrossRef](#)] [[PubMed](#)]
23. Bowker, M. The Role of Precursor States in Adsorption, Surface Reactions and Catalysis. *Top. Catal.* **2016**, *59*, 663–670. [[CrossRef](#)]
24. Nilsson, A.; LaRue, J.; Öberg, H.; Ogasawara, H.; Dell’Angela, M.; Beye, M.; Öström, H.; Gladh, J.; Nørskov, J.; Wurth, W.; et al. Catalysis in real time using X-ray lasers. *Chem. Phys. Lett.* **2017**, *675*, 145–173. [[CrossRef](#)]
25. Wang, H.-Y.; Schreck, S.; Weston, M.; Liu, C.; Ogasawara, H.; LaRue, J.; Perakis, F.; Dell’Angela, M.; Capotondi, F.; Giannessi, L.; et al. Time-resolved observation of transient precursor state of CO on Ru(0001) using carbon K-edge spectroscopy. *Phys. Chem. Chem. Phys.* **2020**, *22*, 2677–2684. [[CrossRef](#)] [[PubMed](#)]
26. LaRue, J.L.; Katayama, T.; Lindenberg, A.; Fisher, A.S.; Öström, H.; Nilsson, A.; Ogasawara, H. THz-Pulse-Induced Selective Catalytic CO Oxidation on Ru. *Phys. Rev. Lett.* **2015**, *115*, 036103. [[CrossRef](#)]
27. Boyd, R.W. The nonlinear optical susceptibility-Chapter 1. In *Nonlinear Optics*; O’Reilly: Sebastopol, CA, USA, 1961; pp. 1–67.
28. Lam, R.K.; Raj, S.L.; Pascal, T.A.; Pemmaraju, C.; Foglia, L.; Simoncig, A.; Fabris, N.; Miotti, P.; Hull, C.J.; Rizzuto, A.M.; et al. Two-photon absorption of soft X-ray free electron laser radiation by graphite near the carbon K-absorption edge. *Chem. Phys. Lett.* **2018**, *703*, 112–116. [[CrossRef](#)]
29. Lam, R.K.; Raj, S.L.; Pascal, T.A.; Pemmaraju, C.D.; Foglia, L.; Simoncig, A.; Fabris, N.; Miotti, P.; Hull, C.J.; Rizzuto, A.M.; et al. Soft X-Ray Second Harmonic Generation as an Interfacial Probe. *Phys. Rev. Lett.* **2018**, *120*, 023901. [[CrossRef](#)]
30. Hoffmann, L.; Jamnuch, S.; Schwartz, C.P.; Helk, T.; Raj, S.L.; Mizuno, H.; Mincigrucci, R.; Foglia, L.; Principi, E.; Saykally, R.J.; et al. Saturable absorption of free-electron laser radiation by graphite near the carbon K-edge. *J. Phys. Chem. Lett.* **2021**, *13*, 39. [[CrossRef](#)]
31. Yamamoto, S.; Omi, T.; Akai, H.; Kubota, Y.; Takahashi, Y.; Suzuki, Y.; Hirata, Y.; Yamamoto, K.; Yukawa, R.; Horiba, K.; et al. Element Selectivity in Second-Harmonic Generation of GaFeO<sub>3</sub> by a Soft-X-Ray Free-Electron Laser. *Phys. Rev. Lett.* **2018**, *120*, 223902. [[CrossRef](#)]
32. Miao, J.; Ercius, P.; Billinge, S.J.L. Atomic electron tomography: 3D structures without crystals. *Science* **2016**, *353*, aaf2157. [[CrossRef](#)]
33. Blanchet, V.; Descamps, D.; Petit, S.; Mairesse, Y.; Pons, B.; Fabre, B. Ultrafast relaxation investigated by photoelectron circular dichroism: An isomeric comparison of camphor and fenchone. *Phys. Chem. Chem. Phys.* **2021**, *23*, 25612–25628. [[CrossRef](#)] [[PubMed](#)]
34. Ilchen, M.; Schmidt, P.; Novikovskiy, N.M.; Hartmann, G.; Rupprecht, P.; Coffee, R.N.; Ehresmann, A.; Galler, A.; Hartmann, N.; Helml, W.; et al. Site-specific interrogation of an ionic chiral fragment during photolysis using an X-ray free-electron laser. *Commun. Chem.* **2021**, *4*, 199. [[CrossRef](#)]
35. Mayer, D.; Lever, F.; Picconi, D.; Metje, J.; Alisaukas, S.; Calegari, F.; Düsterer, S.; Ehlert, C.; Feifel, R.; Niebuhr, M.; et al. Following excited-state chemical shifts in molecular ultrafast x-ray photoelectron spectroscopy. *Nat. Commun.* **2022**, *13*, 198. [[CrossRef](#)] [[PubMed](#)]
36. Faccialà, D.; Devetta, M.; Beauvarlet, S.; Besley, N.; Calegari, F.; Callegari, C.; Catone, D.; Cinquanta, E.; Ciriolo, A.G.; Colaizzi, L.; et al. Time-resolved chiral X-Ray photoelectron spectroscopy with transiently enhanced atomic site-selectivity: A Free Electron Laser investigation of electronically excited fenchone enantiomers. *arXiv* **2022**, arXiv:2202.13704. [[CrossRef](#)]
37. Cerullo, G.; Garavelli, M. A novel spectroscopic window on conical intersections in biomolecules. *Proc. Natl. Acad. Sci. USA* **2020**, *117*, 26553–26555. [[CrossRef](#)] [[PubMed](#)]
38. Keefer, D.; Schnappinger, T.; de Vivie-Riedle, R.; Mukamel, S. Visualizing conical intersection passages via vibronic coherence maps generated by stimulated ultrafast X-ray Raman signals. *Proc. Natl. Acad. Sci. USA* **2020**, *117*, 24069–24075. [[CrossRef](#)]

39. Zinchenko, K.S.; Ardana-Lamas, F.; Seidu, I.; Neville, S.P.; van der Veen, J.; Lanfaloni, V.U.; Schuurman, M.S.; Wörner, H.J. Sub-7-femtosecond conical-intersection dynamics probed at the carbon K-edge. *Science* **2021**, *371*, 489–494. [[CrossRef](#)]
40. Bhattacharjee, A.; Leone, S.R. Ultrafast X-ray Transient Absorption Spectroscopy of Gas-Phase Photochemical Reactions: A New Universal Probe of Photoinduced Molecular Dynamics. *Acc. Chem. Res.* **2018**, *51*, 3203–3211. [[CrossRef](#)]
41. Ross, A.D.; Hait, D.; Scutelnic, V.; Haugen, E.A.; Ridente, E.; Balkew, M.B.; Neumark, D.M.; Head-Gordon, M.; Leone, S.R. Jahn-Teller distortion and dissociation of CCl<sub>4</sub><sup>+</sup> by transient X-ray spectroscopy simultaneously at the carbon K- and chlorine L-edge. *Chem. Sci.* **2022**, *13*, 9310–9320. [[CrossRef](#)]
42. Attar, A.R.; Bhattacharjee, A.; Pemmaraju, C.D.; Schnorr, K.; Closser, K.D.; Prendergast, D.; Leone, S.R. Femtosecond x-ray spectroscopy of an electrocyclic ring-opening reaction. *Science* **2017**, *356*, 54–59. [[CrossRef](#)]
43. Wolf, T.J.A.; Sanchez, D.M.; Yang, J.; Parrish, R.M.; Nunes, J.P.F.; Centurion, M.; Coffee, R.; Cryan, J.P.; Gühr, M.; Hegazy, K.; et al. The photochemical ring-opening of 1,3-cyclohexadiene imaged by ultrafast electron diffraction. *Nat. Chem.* **2019**, *11*, 504–509. [[CrossRef](#)] [[PubMed](#)]
44. Rossos, A.; Kochman, M.; Miller, R.J.D. Ultrafast ring-opening and solvent-dependent product relaxation of photochromic spiroanthopyran. *Phys. Chem. Chem. Phys.* **2019**, *21*, 18119–18127. [[CrossRef](#)]
45. Pertot, Y.; Schmidt, C.; Matthews, M.; Chauvet, A.; Huppert, M.; Svoboda, V.; von Conta, A.; Tehlar, A.; Baykusheva, D.; Wolf, J.-P.; et al. Time-resolved X-ray absorption spectroscopy with a water-window highharmonic source. *Science* **2017**, *355*, 264–267. [[CrossRef](#)]
46. Köppel, H.; Yarkony, D.R.; Barentzen, H. (Eds.) *The Jahn-Teller Effect: Fundamentals and Implications for Physics and Chemistry*; Springer Science & Business Media: Berlin/Heidelberg, Germany, 2009; Volume 97.
47. Mukherjee, S.; Streit, J.K.; Gann, E.; Saurabh, K.; Sunday, D.F.; Krishnamurthy, A.; Ganapathysubramanian, B.; Richter, L.J.; Vaia, R.A.; DeLongchamp, D.M. Polarized X-ray scattering measures molecular orientation in polymer-grafted nanoparticles. *Nat. Commun.* **2021**, *12*, 4896. [[CrossRef](#)] [[PubMed](#)]
48. Stephens, A.D.; Qaisrani, M.N.; Ruggiero, M.T.; Mirón, G.D.; Morzan, U.N.; Lebrero, M.C.G.; Jones, S.T.E.; Poli, E.; Bond, A.D.; Woodhams, P.J.; et al. Short hydrogen bonds enhance nonaromatic protein-related fluorescence. *Proc. Natl. Acad. Sci. USA* **2021**, *118*, e2020389118. [[CrossRef](#)] [[PubMed](#)]
49. Mirian, N.S.; Di Fraia, M.; Spampinati, S.; Sottocorona, F.; Allaria, E.; Badano, L.; Danailov, M.B.; Demidovich, A.; De Ninno, G.; Di Mitri, S.; et al. Generation and measurement of intense few-femtosecond superradiant extreme-ultraviolet free-electron laser pulses. *Nat. Photonics.* **2021**, *15*, 523–529. [[CrossRef](#)]
50. Giannesi, L.; Allaria, E.; Badano, L.; Bencivenga, F.; Callegari, C.; Capotondi, F.; Castronovo, D.; Cinquegrana, P.; Coreno, M.; Danailov, M.B.; et al. FERMI 2.0 UPGRADE STRATEGY. *J. Accel. Conf. Website* **2022**, 1041–1043. [[CrossRef](#)]
51. Nam, Y.; Keefer, D.; Nenov, A.; Conti, I.; Aleotti, F.; Segatta, F.; Lee, J.Y.; Garavelli, M.; Mukamel, S. Conical Intersection Passages of Molecules Probed by X-ray Diffraction and Stimulated Raman Spectroscopy. *J. Phys. Chem. Lett.* **2021**, *12*, 12300–12309. [[CrossRef](#)]
52. Fu, Y.; Nishimura, K.; Shao, R.; Suda, A.; Midorikawa, K.; Lan, P.; Takahashi, E.J. High efficiency ultrafast water-window harmonic generation for single-shot soft X-ray spectroscopy. *Commun. Phys.* **2020**, *3*, 92. [[CrossRef](#)]
53. Jadoun, D.; Kowalewski, M. Time-Resolved Photoelectron Spectroscopy of Conical Intersections with Attosecond Pulse Trains. *J. Phys. Chem. Lett.* **2021**, *12*, 8103–8108. [[CrossRef](#)]
54. Collins, B.A.; Gann, E. Resonant soft X-ray scattering in polymer science. *J. Polym. Sci.* **2022**, *60*, 1199–1243. [[CrossRef](#)]
55. Koliyadu, J.C.P.; Letrun, R.; Kirkwood, H.J.; Liu, J.; Jiang, M.; Emons, M.; Bean, R.; Bellucci, V.; Bielecki, J.; Birnsteinova, S.; et al. Pump-probe capabilities at the SPB / SFX instrument of the European XFEL. *J. Synchrotron Radiat.* **2022**, *29*, 1273–1283. [[CrossRef](#)] [[PubMed](#)]
56. Morzan, U.N.; Videla, P.E.; Soley, M.B.; Nibbering, E.T.J.; Batista, V.S. Vibronic Dynamics of Photodissociating ICN from Simulations of Ultrafast X-Ray Absorption Spectroscopy. *Angew. Chem. Int. Ed.* **2020**, *59*, 20044–20048. [[CrossRef](#)] [[PubMed](#)]
57. Mincigrucci, R.; Kowalewski, M.; Rouxel, J.R.; Bencivenga, F.; Mukamel, S.; Masciovecchio, C. Impulsive UV-pump/X-ray probe study of vibrational dynamics in glycine. *Sci. Rep.* **2018**, *8*, 2–10. [[CrossRef](#)]
58. Ferrario, M.; Alesini, D.; Anania, M.; Artioli, M.; Bacci, A.; Bartocci, S.; Bedogni, R.; Bellaveglia, M.; Biagioni, A.; Bisesto, F.; et al. EuPRAXIA@SPARC\_LAB Design study towards a compact FEL facility at LNF. *Nucl. Instrum. Methods Phys. Res. Sect. A Accel. Spectrometers Detect. Assoc. Equip.* **2018**, *909*, 134–138. [[CrossRef](#)]
59. Pompili, R.; Chiadroni, E.; Cianchi, A.; Ferrario, M.; Gallo, A.; Shpakov, V.; Villa, F. From SPARC\_LAB to EuPRAXIA@SPARC\_LAB. *Instruments.* **2019**, *3*, 45. [[CrossRef](#)]
60. Petrillo, V.; Bacci, A.; Chiadroni, E.; Dattoli, G.; Ferrario, M.; Giribono, A.; Marocchino, A.; Petralia, A.; Conti, M.R.; Rossi, A.; et al. Free Electron Laser in the water window with plasma driven electron beams. *Nucl. Instrum. Methods Phys. Res. Sect. A Accel. Spectrometers Detect. Assoc. Equip.* **2018**, *909*, 303–308. [[CrossRef](#)]
61. Villa, F.; Coreno, M.; Ebrahimpour, Z.; Giannesi, L.; Marcelli, A.; Opromolla, M.; Petrillo, V.; Stellato, F. ARIA—A VUV Beamline for EuPRAXIA@SPARC\_LAB. *Condens. Matter* **2022**, *7*, 11. [[CrossRef](#)]
62. Villa, F.; Balerna, A.; Chiadroni, E.; Cianchi, A.; Coreno, M.; Dabagov, S.A.; Cicco, D.; Gunnella, R.; Marcelli, A.; Masciovecchio, C.; et al. Photon beam line of the water window FEL for the EuPRAXIA@SPARC-LAB project. *J. Phys. Conf. Ser.* **2020**, *1596*, 012039. [[CrossRef](#)]

63. Balerna, A.; Bartocci, S.; Batignani, G.; Cianchi, A.; Chiadroni, E.; Coreno, M.; Cricenti, A.; Dabagov, S.; Di Cicco, A.; Faiferri, M.; et al. The potential of eupraxia@sparc\_lab for radiation based techniques. *Condens. Matter* **2019**, *4*, 30. [[CrossRef](#)]
64. Guyader, L.L.; Eschenlohr, A.; Beye, M.; Schlotter, W.; Döring, F.; Carinan, C.; Hickin, D.; Agarwal, N.; Boeglin, C.; Bovensiepen, U.; et al. Photon shot-noise limited transient absorption soft X-ray spectroscopy at the European XFEL. *arXiv* **2022**. [[CrossRef](#)]
65. Gerasimova, N.; La Civita, D.; Samoylova, L.; Vannoni, M.; Villanueva, R.; Hickin, D.; Carley, R.; Gort, R.; Van Kuiken, B.E.; Miedema, P.; et al. The soft X-ray monochromator at the SASE3 beamline of the European XFEL: From design to operation. *J. Synchrotron Radiat.* **2022**, *29*, 1299–1308. [[CrossRef](#)] [[PubMed](#)]
66. Mazuritskiy, M.I.; Lerer, A.M. Focusing of Long-Wavelength X-Rays by Means of Spherical and Planar Microchannel Plates. *JETP Lett.* **2020**, *112*, 138–144. [[CrossRef](#)]
67. Mazuritskiy, M.I.; Lerer, A.M.; Marcelli, A.; Dabagov, S.B.; Coreno, M.; D’Elia, A.; Rezvani, S.J. Wave propagation and focusing of soft X-rays by spherical bent microchannel plates. *J. Synchrotron Radiat.* **2021**, *28*, 383–391. [[CrossRef](#)] [[PubMed](#)]
68. Mazuritskiy, M.I.; Lerer, A.M.; Dabagov, S.B.; Marcelli, A. Coherent X-ray Fluorescent Excitation inside MCP Microchannels: Axial Channeling and Wave Propagation. *J. Surf. Investig.* **2021**, *15*, 513–519. [[CrossRef](#)]
69. Mazuritskiy, M.I.; Lerer, A.M.; Marcelli, A.; Dabagov, S.B. Synchrotron radiation transmission by two coupled flat microchannel plates: New opportunities to control the focal spot characteristics. *J. Synchrotron Radiat.* **2022**, *29*, 355–362. [[CrossRef](#)]
70. Schulz, J.; Bielecki, J.; Doak, R.B.; Dörner, K.; Graceffa, R.; Shoeman, R.L.; Sikorski, M.; Thute, P.; Westphal, D.; Mancuso, A.P. A versatile liquid-jet setup for the European XFEL. *J. Synchrotron Radiat.* **2019**, *26*, 339–345. [[CrossRef](#)]
71. Kirian, R.A.; Awel, S.; Eckerskorn, N.; Fleckenstein, H.; Wiedorn, M.; Adriano, L.; Bajt, S.; Barthelmess, M.; Bean, R.J.; Beyerlein, K.R.; et al. Simple convergent-nozzle aerosol injector for single-particle diffractive imaging with X-ray free-electron lasers. *Struct. Dyn.* **2015**, *2*, 041717. [[CrossRef](#)]
72. Klein, Y.; Strizhevsky, E.; Capotondi, F.; de Angelis, D.; Giannessi, L.; Pancaldi, M.; Pedersoli, E.; Penco, G.; Prince, K.C.; Sefi, O.; et al. High-resolution absorption measurements with free-electron lasers using ghost spectroscopy. *arXiv* **2022**, arXiv:2203.00688. [[CrossRef](#)]
73. Driver, T.; Li, S.; Champenois, E.G.; Duris, J.; Ratner, D.; Lane, T.J.; Rosenberger, P.; Al-Haddad, A.; Averbukh, V.; Barnard, T.; et al. Attosecond transient absorption spooktscopy: A ghost imaging approach to ultrafast absorption spectroscopy. *Phys. Chem. Chem. Phys.* **2020**, *22*, 2704–2712. [[CrossRef](#)]